EVS29 Symposium
Montréal, Québec, Canada, June 19 - 22, 2016

Energy Optimal Operation of Hybrid Battery Systems and Comparison to a Single-Cell Reference System for Electric Vehicles Including the Aged State of High Energy Cells

Raphael Wegmann[1,2], Volker Döge[2], Dirk Uwe Sauer[3,4]
[1]*Corresponding author, raphael.wegmann@de.bosch.com*
[2]*Corporate Sector Research and Advance Engineering, Robert Bosch GmbH, 71272 Renningen, Germany*
[3]*Institute for Power Electronics and Electrical Drives (ISEA), RWTH Aachen University, 52066 Aachen, Germany*
[4]*Jülich Aachen Research Alliance, JARA-Energy, Germany*

Abstract

In battery electric vehicles the battery system has to satisfy demanding requirements. On the one hand, high power capabilility has to be provided for varying states of charge and temperature. On the other hand, the battery system should achieve a maximum service life, optimal energy efficiency and a high overall driving range. This paper compares a conventional single-cell battery system with two hybrid battery system topologies that aim at improving the mentioned aspects of the conventional system. The hybrid battery systems each comprise two battery parts connected via a dc-to-dc converter, one part including lithium-ion battery cells optimized for high energy density and the other part equipped with high power density type lithium-ion cells. An optimal control problem is formulated and solved with Dynamic Programming. The mentioned topologies are then compared in terms of energy efficiency, power capability and current distribution. A real life driving cycle power demand is used for this comparison. It can be shown that the hybrid battery system reduces the occurrence of high current rates on the high energy battery part and shows better energy efficiency when operated with aged high energy battery cells. Furthermore the hybrid battery system's potential to obtain a high power capability in low state of charge regions is shown.

Keywords: BEV (battery electric vehicle), lithium battery, power management, energy consumption, cycle life

1 Introduction

An increasing internal resistance, capacity fade and the scalability of power and energy requirements are challenges in battery system design and operation. Additionally, a decreasing power capability at low/high states of charge (SoC) or low temperatures has to be expected. The battery system is the main cost factor within the vehicle's powertrain [13, 23]. To cope with these problems one can find a hybrid battery system topology in literature, combining a high energy and a high power storage part. Gao et al. and Holland et al. [10, 15] address a passive parallel connection of two different energy storage parts. An active hybrid battery system, combining the energy storage parts via a dc-to-dc converter, introducing a simple load sharing strategy for traction applications can be found in [2, 5], for example.

Other targets that can be linked to a hybrid battery system are the enhancement of power capability and energy efficiency in Plug-in Electric Vehicles [8, 20]. On top of that, the hybrid system makes recuperation possible for Fuel Cell Electric Vehicles [28], and provides advantages in terms of power capability [28] and scalability [24]. For Hybrid Fuel Cell and Hybrid Electric Vehicles, optimization problems that can be solved off-line via dynamic programming, are formulated and solved in [1, 17, 19]. In this paper, an optimal control problem minimizing battery power losses for two hybrid battery system topologies is formulated and solved. The behavior and performance of these topologies is then compared to a single-cell battery system for a specified vehicle and driving cycle scenario.

2 Battery System Topologies for Electric Vehicles

2.1 Comparison of Battery Topologies

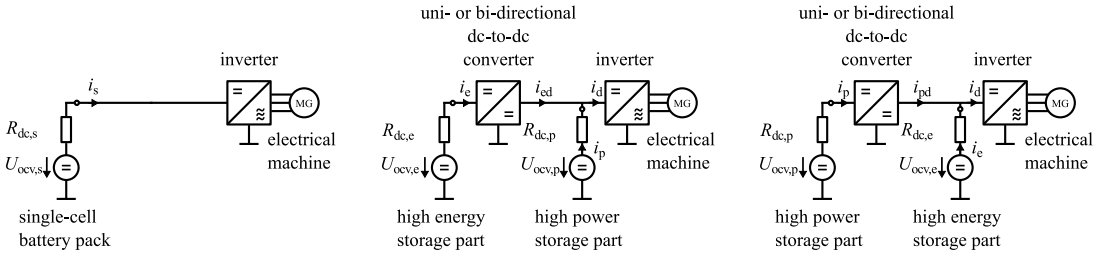

(a) Single-cell battery system

(b) Hybrid battery system topology 1

(c) Hybrid battery system topology 2

Figure 1: Investigated battery system topologies within the powertrain for a full electric vehicle.

The investigated powertrain topologies are shown in figure 1. The single-cell battery pack system, that can mostly be found in today's electric cars, e. g. Tesla Model S, Fiat 500e or BMW i3 is shown in figure 1a. It comprises one type of battery cells within the energy storage system. In contrast the hybrid battery system topologies, shown in figure 1b and 1c, comprise a high energy and a high power storage part that is equipped with a high energy density and a high power density battery cell respectively.

When integrating the hybrid battery system into the powertrain there are several possibilities. The interconnection of the two battery parts itself can be done via a direct parallel connection or an actively controlled connection via dc-to-dc converter. Additional power electronics can be saved for the direct parallel connection but there is no possibility to individually control the currents. When operating this hybrid battery system topology high attention has to be devoted to the current, temperature and voltage limits of the individual battery cells. Connecting the storage parts with a uni- or bi-directional dc-to-dc converter [7] allows for an individual usage of the two battery parts and leads ultimately to the possibility to optimize the power distribution in terms of a defined objective. The latter is addressed here.

An additive dc-to-dc converter, connecting either the single-cell or the hybrid battery system to the traction inverter would allow for an operation of the inverter within an optimal input voltage window but leads to additional system cost and an increase in system weight and volume [11, 27]. Here, the dc-to-dc converter is considered with an efficiency map, derived from a resonant traction converter topology. Furthermore the efficiencies of the inverter and the electrical machine are stored in a data map containing the efficiencies in dependence of machine torque, machine speed and the inverter input voltage at the dc-link.

2.2 Characterization of High Energy and High Power Storages

The basic characteristics of the two chosen battery cells for the hybrid battery system are shown in table 1. The high energy cell contains a nickel cobalt aluminium oxide (NCA) material for the cathode and graphite as anode material. In contrast to that, the anode material of the high power cell is lithium titanate (LTO), and the cathode contains a transition metal oxide active material.

Depending on the problem that has to be solved, a balance between accuracy, time and memory consuming requirements has to be found when modeling the battery behavior. Because of the optimization method proposed in section 3, a battery model based on a voltage source and an ohmic resistance is chosen in this work as it can be seen in figure 1 for the different battery system topologies. The voltage

Table 1: Characteristics of the high energy and high power battery cells. The Begin of Life (BoL) data refers to the nominal cell data and the End of Life (EoL) parameters refer to a cycled cell, whose approach on reaching EoL and measurements are explained in section 2.3. Specific power is calculated at the stated C-rate.

Cell type	High energy cell (BoL)	High energy cell (EoL)	High power cell (BoL)
Available Capacity	3.18 Ah	2.62 Ah	6 Ah
Upper voltage limit	4.2 V	4.2 V	2.7 V
Low voltage limit	2.5 V	2.5 V	1.5 V
Specific energy	240 Wh/kg	199 Wh/kg	63 Wh/kg
Specific discharge power (SoC 50 %, 23 °C)	454 W/kg (2 C)	414 W/kg (2 C)	2100 W/kg (40 C)

source represents the open circuit voltage (OCV) depending on the battery's state of charge, whereas the resistance R_{dc} models the cell's direct current resistance (DCR), depending on state of charge, the battery's temperature and current direction, i. e. either the discharge direct current resistance $R_{\mathrm{dc,dch}}$ or the charge current resistance $R_{\mathrm{dc,ch}}$. The open circuit voltage curves for the two cells were measured at room temperature using a relaxation measurement [26]. Thus the cells were fully charged and gradually discharged with small and short current pulses followed by a long rest period to reach nearly equilibrium voltage. This procedure was repeated until the lower voltage limit was reached. The direct current resistance values were measured using another current pulse characterization method [14, 26]. To this end the voltage response following from a 10 s current pulse was measured for different SoC and temperature steps and for both charging and discharging currents.

2.3 Comparison of Begin of Life and End of Life Performance

From the determined DCR and OCV maps illustrated in the previous section the immediate voltage response caused by a current load can be modeled using equation (1). A positive current is defined here as the discharge direction.

$$U_{\mathrm{bat}}(\mathrm{SoC}, T) = U_{\mathrm{ocv}}(\mathrm{SoC}) - R_{\mathrm{dc}}(\mathrm{SoC}, T, \text{current direction}) \cdot I_{\mathrm{bat}} \tag{1}$$

Using this battery model and additional information, the power capability of the respective battery cell can be estimated, as it is explained in the following.

The battery manufacturer usually provides information of temperature dependent voltage and current limits for a specific cell, i. e. the upper and lower voltage limits $U_{\max}(T)$ and $U_{\min}(T)$. Also charge and discharge current limits $I_{\mathrm{min,ch}}(T)$ and $I_{\mathrm{max,dch}}(T)$ are provided. Alternatively the charge and discharge current limits can be well defined for a specific application. Furthermore an upper and lower operation temperature limit is given. Together with the DCR maps, estimated in the manner explained before, the theoretical maximum discharge and minimum charge current $I_{\mathrm{max,dch,bound}}(\mathrm{SoC}, T)$ and $I_{\mathrm{min,ch,bound}}(\mathrm{SoC}, T)$, which would cause the voltage to reach its lower or upper voltage limit immediately, can be estimated for different temperature and SoC operating points, see equations (2) and (3).

$$I_{\mathrm{max,dch,bound}}(\mathrm{SoC}, T) = \frac{U_{\mathrm{ocv}}(\mathrm{SoC}) - U_{\min}(T)}{R_{\mathrm{dc,dch}}(\mathrm{SoC}, T)} \qquad \text{Theoretical maximum discharge current} \tag{2}$$

$$I_{\mathrm{min,ch,bound}}(\mathrm{SoC}, T) = \frac{U_{\mathrm{ocv}}(\mathrm{SoC}) - U_{\max}(T)}{R_{\mathrm{dc,ch}}(\mathrm{SoC}, T)} \qquad \text{Theoretical minimum charge current} \tag{3}$$

Due to the usage of a DCR based on the voltage response after some seconds, the calculated current limits (2) and (3) are conservative for loads that appear in frequency range above 1/10 s. By comparison, loads occurring with a lower frequency like diffusion processes would be modeled with too low overvoltages. For automotive applications the DCR within a time scale of 10 s shows an adequate order of magnitude for calculating the power capabilities in dynamic driving cycles.

The global current limits, including the mentioned theoretical current limits and the temperature dependent current limits given by the battery manufacturer or defined in dependence of the application, can be estimated as shown in equation (4) and (5).

$$I_{\mathrm{max,dch,global}}(\mathrm{SoC}, T) = \min(I_{\mathrm{max,dch,bound}}(\mathrm{SoC}, T), I_{\mathrm{max,dch}}(T)) \quad \text{Global discharge current} \quad (4)$$

$$I_{\mathrm{min,ch,global}}(\mathrm{SoC}, T) = \max(I_{\mathrm{min,ch,bound}}(\mathrm{SoC}, T), I_{\mathrm{min,ch}}(T)) \quad \text{Global charge current} \quad (5)$$

The power capabilities can then be calculated using ohmic's law and the stated calculations. The maximum discharge power at a given SoC and battery temperature is shown in equation (6), the minimum charging power is displayed in equation (7) respectively. Electrical losses occurring in the battery are reflected by the second term $R_{\mathrm{dc}} \cdot I^2$ in each of these two equations.

$$P_{\mathrm{max,dch}}(\mathrm{SoC}, T) = U_{\mathrm{ocv}}(\mathrm{SoC}) \cdot I_{\mathrm{max,dch,global}} - R_{\mathrm{dc,dch}}(\mathrm{SoC}, T) \cdot I^2_{\mathrm{max,dch,global}} \quad (6)$$

$$P_{\mathrm{min,ch}}(\mathrm{SoC}, T) = U_{\mathrm{ocv}}(\mathrm{SoC}) \cdot I_{\mathrm{min,ch,global}} - R_{\mathrm{dc,ch}}(\mathrm{SoC}, T) \cdot I^2_{\mathrm{min,ch,global}} \quad (7)$$

Lithium-ion batteries show a decrease in available capacity and an increase in the DCR over lifetime due to aging mechanisms [6, 32]. In literature the terms begin of life (BoL) and end of life (EoL) can be found. Especially EoL is a soft term that defines the moment within the battery's lifetime where it should not be used anymore in its specific application. EoL can refer to a loss of capacity, a loss in power capability or it can be a definition combining both of these criteria. For a battery electric vehicle, EoL of the battery cell is often defined for the moment where the cell's actual capacity reaches $80\,\%$ of the nominal cell capacity at BoL [16, 22, 31].

In order to compare the performance of the proposed battery system topologies the static power capability maps for the high power and the high energy battery cell were calculated using the measured DCR and OCV parameters and the method described previously.

Additional attention is given to the EoL performance of the high energy battery cell here. Therefore a cell was cycled until meeting the end of life criteria. In fact the cell reached an available capacity of around $82\,\%$ of the nominal begin of life capacity at the end of the cycling test. Testing was done in a climate chamber with an ambient temperature of $23\,^{\circ}\mathrm{C}$. The cell was charged with a constant charge current of a $0.5\,\mathrm{C}$ rate until reaching the upper voltage limit $4.1\,\mathrm{V}$, then it was immediately discharged with a $1\,\mathrm{C}$ rate until reaching the lower boundary limit of $2.5\,\mathrm{V}$. This cycle profile was repeated periodically. After this test the OCV and DCR parameters were measured with the previously mentioned pulse tests. The derived power capabilities of the high energy cell for BoL and EoL conditions are shown in figure 2. The defined maximum discharge current limit is set to $8\,\mathrm{A}$. Two effects can be seen: For both the BoL and EoL condition, the discharge power capability is strongly decreasing in low SoC regions. This is on the one hand affected due to the closeness of cell voltage and lower voltage limit. On the other hand the DCR in either charge or discharge direction is strongly increasing with decreasing SoC. This leads to higher overvoltages within the cell and thus to a lower possible discharge current as stated in equation (2).

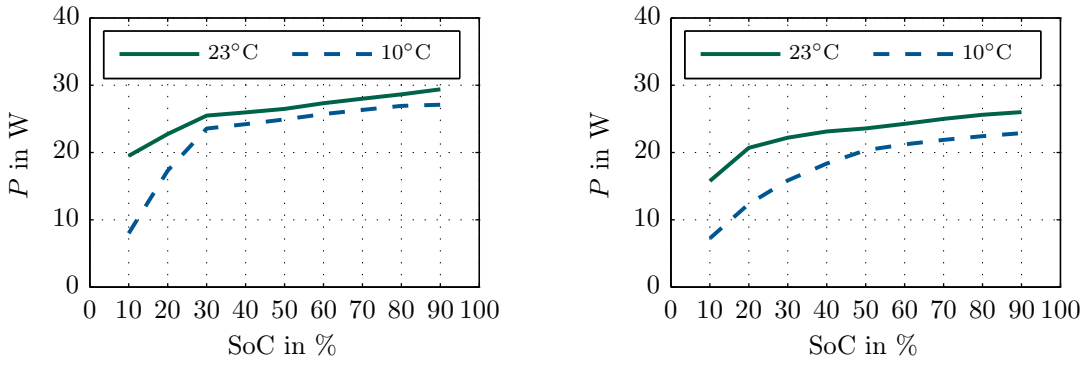

(a) Begin of Life **(b)** End of Life

Figure 2: Results of the stated measurements and calculations: Discharge power capabilities of the high energy cell for two temperatures; used in this work for begin of life (BoL) as well as end of life (EoL) condition. The SoC scale in the two figures is related to the respective actual capacity.

Comparing the lifetime conditions, the DCR in discharge direction at SoC $50\,\%$ and $23\,^{\circ}\mathrm{C}$ is increasing by factor $R_{\mathrm{dc,dch}}(50\,\%,\mathrm{EoL})/R_{\mathrm{dc,dch}}(50\,\%,\mathrm{BoL}) = 2.06$. A similar behavior can be found for the charge

direction where the ratio $R_{\mathrm{dc,ch}(50\,\%,\mathrm{EoL})}/R_{\mathrm{dc,dch}(50\,\%,\mathrm{BoL})} = 1.86$ arises. This will later be reflected in an occurrence of higher electrical energy losses within the battery and a loss in discharge capability for a low SoC range for the EoL scenarios.

3 Optimal Power Management Strategy using Dynamic Programming

A hybrid battery system offers the degree of freedom of distributing the electrical propulsion power demand to two or even more storage parts, under the condition of meeting all boundary conditions, e. g. current, voltage and temperature limits. Hence there are several objectives the power management could pursue to overcome the restrictions of conventional single-cell battery systems that have been explained before. Maximizing the discharge and/or charge power capability, minimizing the overall electrical energy losses in the powertrain or maximizing the battery's lifetime could be objectives. Either one of the mentioned objectives or a combination of several objectives, linked with weighting factors, are conceivable. Here the objective of minimizing the overall electrical energy losses within the powertrain is investigated.

To include nonlinearities of the investigated powertrain system and several boundary conditions in the optimal control problem formulation, an adequate optimization algorithm is needed. A Dynamic Programming algorithm fulfills the mentioned requirements and is briefly outlined in the following. Subsequently an optimal control problem for the hybrid battery system is formulated that will be solved using a Deterministic Dynamic Programming algorithm as presented in [29]. To use the subsequently introduced algorithm the system's dynamic equations have to be discretized. Both the disturbance w_k and the resulting state and control trajectories are discretized. The optimal control problem's nature can be a stochastic or a deterministic one [4]. The problems investigated here have a finite time horizon and their disturbance, i. e. the driving cycle, is known in advance. The discrete time step sizes Δt are equal over the whole time horizon $t(k) = k \cdot \Delta t$, considering $k \in \{0, 1, \ldots, N-1\}$. Solving these problems via Dynamic Programming is outlined in the following.

3.1 Dynamic Programming

A general formulation of an optimal control problem is given in equations (8) to (14). It is the objective to minimize a cost J that occurs over time and is additive for all time steps [4]. In dependence of the initial state $\underline{x}_0$ the total cost for the problem is shown in equation (9). The so called Mayer term $g_N(x_N)$ represents the cost in the last time step N [9, 18]. In cases where a specific final state, respectively specific final states $\underline{x}(N)$ shall be reached, a penalty term can be added to the performance index J_π, that leads to a big cost due to violating the final state criteria [12, 30]. The dynamic system according to equation (10) expresses the evolution of state variables from one to the following discrete time step for $k = 0, 1, \ldots N$-1 [4].

$$\min_{\{\forall k:\ \underline{x}_k \in \mathcal{X}_k, \underline{u}_k \in \mathcal{U}_k\}} J_\pi(\underline{x}, \underline{u}) \tag{8}$$

$$J_\pi(\underline{x}, \underline{u}) := g_N(\underline{x}_N) + \sum_{k=0}^{N-1} g_k(\underline{x}_k, \underline{u}_k, w_k) \tag{9}$$

s.t.

$$\underline{x}_{k+1} = \underline{x}_k + \underline{f}(\underline{x}_k, \underline{u}_k, w_k) \tag{10}$$

$$\underline{x}_k \in \mathcal{X}_k \subseteq \mathbb{R}^n \tag{11}$$

$$\underline{u}_k \in \mathcal{U}_k \subseteq \mathbb{R}^m \tag{12}$$

$$\underline{x}(0) = \underline{x}_0 \tag{13}$$

$$\underline{x}(N) \in [\underline{x}_{N,min}, \underline{x}_{N,max}] \tag{14}$$

The state evolution at each time step k depends on the control input $\underline{u}_k$ and the actual disturbance w_k, that is known in advance here. In equation (13) and (14) the initial conditions of the state variables and the boundary conditions in the last time step N are shown, respectively. The objective of the formulated control problem is to find an optimal control policy given by $\pi^* = \{\underline{u}_0^*, \underline{u}_1^*, \ldots, \underline{u}_{N-1}^*\}$ that globally minimizes a given objective functional (9) [18].

Dynamic Programming refers to a method that allows to solve optimal control problems like the one previously described under certain circumstances. It is based on the principle of optimality defined by Richard Bellman:

> *"An optimal policy has the property that whatever the initial state and initial decision are, the remaining decisions must constitute an optimal policy with regard to the state resulting from the first decision."* [3]

This principle implies that wherever on the optimal control route $\pi^* = \{\underline{u}_0^*, \underline{u}_1^*, \ldots, \underline{u}_{N-1}^*\}$ of the whole problem a state $\underline{x}_k$ at time step $k \in [0, N-1]$ is reached, the optimal control policy from that specific state on, i. e. $\pi^*(\underline{x}_k) = \{\underline{u}_k^*, \underline{u}_{k+1}^*, \ldots, \underline{u}_{N-1}^*\}$, will also lie on the rest of the optimal control route for the whole problem.
A Dynamic Programming algorithm solves the underlying problem sequentially by reducing it to subproblems that are solved going backwards in time [4]. This is stated by the recursive formulation (15), also called Bellman equation or cost-to-go function [12, 29]. Starting from a final state $\underline{x}_N$ with terminal cost $g_N(\underline{x}_N)$, the optimal cost at every state $\underline{x}_k$ is calculated based on the optimal cost at the next step $k+1$ that has already been determined and the optimal control variable $\underline{u}_k$ that can be applied at the current step. In this manner the problem will be solved recursively.

$$J_k^*(\underline{x}_k) = \min_{\{\forall k:\, \underline{x}_k \in \mathcal{X}_k, \underline{u}_k \in \mathcal{U}_k\}} \{g_\mathrm{k}(\underline{x}_k, \underline{u}_k) + J_{k+1}^*(\underline{x}_{k+1})\} \tag{15}$$

3.2 Optimal Control Problem Formulation for the Hybrid Battery System

In figure 3 the powertrain simulation within the Dynamic Programming optimization is outlined. The index numbers of the batteries in the figure refer to the battery parts of the corresponding hybrid battery system topology mentioned in 2.1. When topology one is chosen, index 1 refers to the high power battery part and index 2 refers to the high energy battery part. For the second hybrid battery system topology this assignment is vice versa. For a given driving cycle, i. e. a velocity and gradient profile over time, and given vehicle parameters, the traction force that is required to propel the vehicle can be calculated for each moment in time according to a longitudinal dynamics equation. Then the power to propel the electric vehicle, for a given time step k can be calculated from the torque-speed relationship at the wheel $P_{\mathrm{propulsion,k}} = M_{\mathrm{w,k}} \cdot \omega_{\mathrm{w,k}}$. For a deeper insight into the outlined calculations the reader is referred to [12].

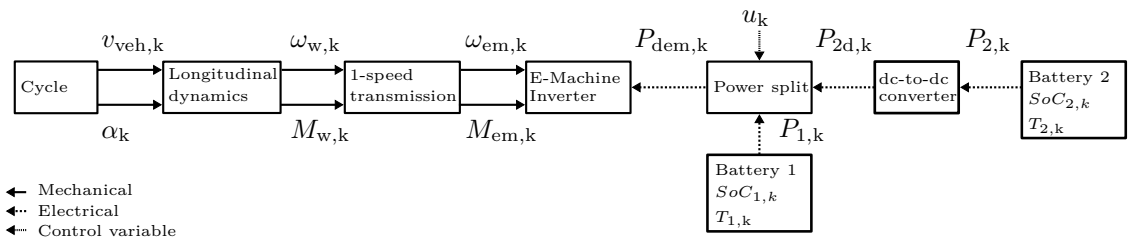

Figure 3: Electric vehicle powertrain with hybrid battery system within the context of Dynamic Programming.

Besides the mentioned propulsion power the battery parts have to provide additive power that occurs in form of electrical losses within the different powertrain components. These losses include losses in the two battery parts themselves $P_\mathrm{loss,e}$ and $P_\mathrm{loss,p}$, the dc-to-dc converter $P_\mathrm{loss,dcdc}$ and the dc-to-ac inverter plus the electrical machine losses $P_\mathrm{loss,invem}$. Equation (16) is reflecting this power relationship. The two terms on the left side of the equal sign reflect the net power occurring in the respective battery part. The electrical losses in the battery parts $P_\mathrm{loss,e}$ and $P_\mathrm{loss,p}$ are reflected by the DCR-current-relationship $R_\mathrm{dc} \cdot I^2$ as in equations (6) and (7).

$$U_\mathrm{ocv,e} \cdot i_\mathrm{e} + U_\mathrm{ocv,p} \cdot i_\mathrm{p} = P_\mathrm{loss,e} + P_\mathrm{loss,p} + P_\mathrm{loss,dcdc} + P_\mathrm{loss,invem} + P_\mathrm{propulsion} \tag{16}$$

The objective investigated here is the minimization of the overall electrical energy losses within the powertrain for a given driving cycle. The corresponding cost function J_π is described in equation (17). Due to the fact that the discrete time steps Δt are equal over the whole time horizon $t(k) = k \cdot \Delta t$, a multiplication of the electrical power losses with time step Δt can be omitted. Losses occurring in the

1-speed transmission are neglected. In section 3.1 the principle approach of Dynamic Programming is explained. Here the Deterministic Dynamic Programming algorithm introduced in [29] is used to solve the given control problem.

$$J_\pi(\underline{x}_k, \underline{u}_k) = \sum_{k=0}^{N-1} U_{\mathrm{ocv,p}}(\underline{x}_k) \cdot i_p(\underline{x}_k, \underline{u}_k) + U_{\mathrm{ocv,e}}(\underline{x}_k) \cdot i_e(\underline{x}_k, \underline{u}_k) \tag{17}$$

To solve the problem the one-dimensional control variable $u(k)$ is defined that influences the power share between battery part one P_1 and battery part two $P_{2\mathrm{d}}$ at the side of the dc-link. The relationship is given in equation (18) and (19). A so called power split offset pso has been defined, to enable a power flow between the two battery parts in times when no power P_{dem} is demanded. It is a constant value with the physical unit Watt.

$$P_1(k) = u(k) \cdot P_{\mathrm{dem}}(k) + u(k) \cdot pso \tag{18}$$

$$P_{2\mathrm{d}} = (1 - u(k)) \cdot P_{\mathrm{dem}}(k) - u(k) \cdot pso \tag{19}$$

The states of charge and the temperatures of the two battery parts define the state variables stated in vector $\underline{x}_k = [\mathrm{SoC}_{1,k}, T_{1,k}, \mathrm{SoC}_{2,k}, T_{2,k}]^{\mathrm{T}}$. The resulting state of charge $\mathrm{SoC_j}(k+1)$ of the respective battery in time step $k+1$, in dependence of the former state of charge $\mathrm{SoC}(k)$, the battery current $I_{\mathrm{j}}(k)$, the total available capacity $Q_{\mathrm{j,TAC}}$ and time step Δt, is given in equation (20).

$$\mathrm{SoC_j}(k+1) = \mathrm{SoC_j}(k) - \Delta t \cdot \frac{I_{\mathrm{j}}(k)}{Q_{\mathrm{j,TAC}}} \qquad \mathrm{j} \in \{1, 2\} \tag{20}$$

Corresponding to the SoC evolution the temperature evolution is given in equation (21). The generated energy per unit of time, i. e. the heat flow $\dot{Q}_{\mathrm{j,gen}}(k)$ is reflected by joule heating due to electrochemical polarization and pure ohmic losses [21]. The dissipated heat from the battery per unit of time $\dot{Q}_{\mathrm{j,diss}}(k)$ is reflected here by a term considering the heat convection and a heat radiation term according to the Stefan-Boltzmann Law [26].

$$T_{\mathrm{j}}(k+1) = T_{\mathrm{j}}(k) + \frac{\Delta t}{m_{\mathrm{j}} \cdot c_{\mathrm{j,th}}} \cdot (\dot{Q}_{\mathrm{j,gen}}(k) - \dot{Q}_{\mathrm{j,diss}}(k)) \qquad \mathrm{j} \in \{1, 2\} \tag{21}$$

The battery current $I_{\mathrm{j},k}$ for the states $\underline{x}_k$ and the control variable u_k can be calculated according to equation (22).

$$I_{\mathrm{j},k}(\underline{x}_k, u_k) = \frac{U_{\mathrm{ocv,j},k} - \sqrt{U^2_{\mathrm{ocv,j},k} - 4 \cdot R_{\mathrm{dc,j},k} \cdot P_{\mathrm{j},k}}}{2 \cdot R_{\mathrm{dc,j},k}} \qquad \mathrm{j} \in \{1, 2\} \tag{22}$$

Several constraints were implemented in the optimization environment. Time invariant constraints are given for the temperature boundaries according to manufacturer data, for the peak power of the dc-to-dc converter and for the maximum electrical machine speed. Furthermore the states of charge may only occur in the range 0 % to 100 %. Time variant constraints are calculated in every time step in dependence of the states and include the charging and discharging power limits mentioned in section 2.3 and the maximum electrical machine torque.

4 Results and Discussion

4.1 Investigated Scenarios

In this work simulations and Dynamic Programming optimizations are done for a single-cell and two hybrid battery system designs as proposed in section 2. To get an insight into the electric vehicle's performance at different stages of the high energy battery lifetime, an investigation for the proposed topologies is done with a high energy battery at BoL and EoL. The maximum discharge and charge current rate on the high power battery part was limited to a 1 C rate.

To compare the three mentioned topologies the same overall energy for each battery system is chosen. The high energy battery part of the hybrid battery system topologies comprises 23.56 kWh and the high power battery part 2.24 kWh electrical energy. The single-cell battery pack contains an overall energy of 25.8 kWh.

The World Harmonized Light-Vehicles Test Cycle (WLTC, class 3) is chosen in this work. It comprises driving patterns with low, mid and high velocity patterns, up to a maximum velocity of 131.3 km/h [25]. To use a large amount of the battery system's energy a long distance drive with the electric vehicle is investigated. Therefore the cycle is repeated until a distance of 170 km is reached. Simulations are done for an ambient temperature of 23 °C.

4.2 Results of the Single-cell and Hybrid Battery System Scenarios

The different shares of electrical energy losses for the powertrain components are displayed in figure 4. When comparing the single-cell battery system with the hybrid battery system topologies, for the BoL scenario, it is noted that the overall electrical energy losses in the powertrain of the hybrid battery system topologies are higher. This is mainly due to the additive dc-to-dc converter losses. In contrast a comparison of the EoL scenarios shows that the overall electrical energy losses in the powertrain of the single-cell battery exceed the ones in the hybrid battery system powertrain topologies. For the hybrid battery system topologies electrical losses in the high energy battery can be limited by shifting load to the high power battery part. These increased losses can not be avoided in the aged battery of the single-cell battery system since it has to provide the demanded power.

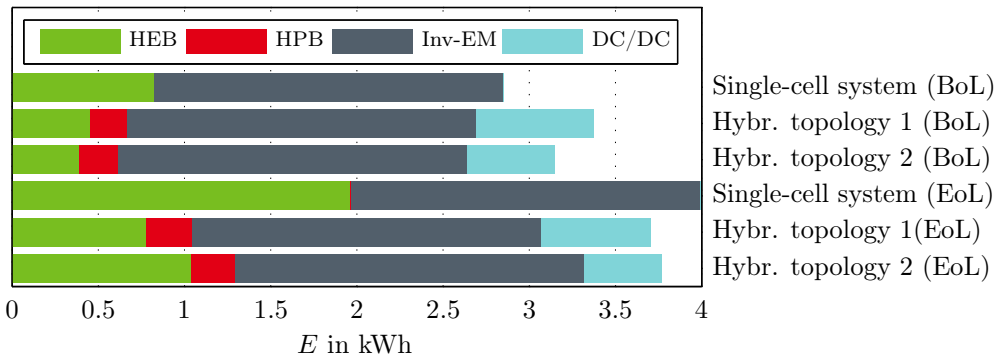

Figure 4: Electrical energy losses within the powertrain for the three battery system topologies. The losses occur for the whole driving cycle mentioned in 4.1. The upper three bar plots represent the battery system topologies with an integrated high energy battery at BoL condition, the lower three bar plots represent the topologies with a high energy battery that have reached EoL condition respectively. Losses refer to those in the high energy battery part, respectively single-cell battery pack (HEB), high power battery part (HPB), inverter and electrical machine (Inv-EM) and dc-to-dc converter (DC/DC).

A comparison of the net absolute energy throughput on cell level for the high energy cell, i. e. $E_{\mathrm{net,cell}} = \sum_{k=0}^{N-1} U_{\mathrm{ocv,cell}}(k) \cdot |I_{\mathrm{cell}}(k)| \cdot \Delta t$, shows that the throughput on the energy cells of the hybrid battery topologies is much smaller than the throughput on the high energy cells of the single-cell battery system. For example the hybrid battery system topologies 1 and 2 show a throughput of 9.89 Wh respectively 9.81 Wh on one high energy cell in the BoL scenario, whereas the single-cell system shows a throughput of 14.75 Wh.Similar results arise from the EoL scenarios, here the throughput for the high energy cells of the hybrid battery system is 9.26 Wh for topology 1, respectively 12.51 Wh for topology 2, whereas the single-cell battery system has a throughput of 15.06 Wh. The latter comparison shows a reduction of net energy throughput on the high energy cells of up to 38.5 % when operating the hybrid battery system in comparison to the single-cell system.

4.3 Single-cell Battery System Results

First the single-cell battery system results for the BoL and the EoL scenario are discussed. In figure 5 the driving cycle's velocity profile and the SoC trajectories of the single-cell battery system topology for BoL and EoL conditions are shown. It can be seen that the EoL scenario reaches a lower final SoC due to the reduced battery capacity for the aged cell and higher electrical energy losses that will be discussed subsequently. Figure 6 shows a comparison of the net energy throughput related to the C rate for the BoL

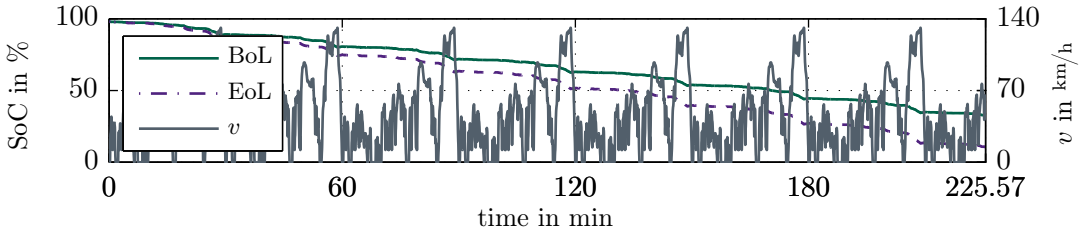

Figure 5: Single-cell battery system SoC trajectories for the BoL and EoL scenarios. Velocity trajectory of the repeated WLTC driving cycle.

and the EoL scenario. It can be observed that the overall discharged net energy from the battery increases from BoL to EoL scenario. For the recuperated energy the opposite is true, the overall recuperated net energy decreases from BoL to EoL scenario. This is due to the increasing inner resistance of the cell and the changing course of the open circuit voltage U_{ocv}. On the EoL battery, the U_{ocv} decreases faster when taking the same net energy from the battery, what in turn leads to increasing currents too and is thereby additionally raising the electrical battery losses. When taking energy from the cell to propel the vehicle, higher energy battery losses have to be made up for. When doing a regenerative braking phase, less net recuperation energy can be stored in the battery due to higher electrical losses. The fact of increasing current stress on the battery for the EoL condition can be seen in figure 6b. The peak current rate reaches a rate of about 2 C. Here the C rate is related to the battery's capacity at begin of life. Besides the increase in electrical losses the increase in current rates also leads to an additive temperature generation.

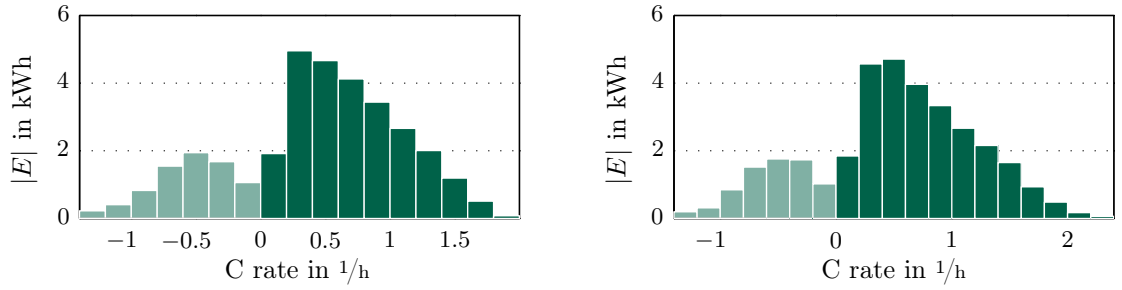

(a) Begin of Life

(b) End of Life

Figure 6: Energy throughput on the single-cell battery system for BoL and EoL condition of the high energy battery, related to the C rate (C rate > 0; Discharge).

4.4 Dynamic Programming Results for the Hybrid Battery System

To get an insight into the optimization results of the hybrid battery system scenarios mentioned in section 4.1, figure 7 shows an excerpt of a result. It displays the split of the power demand P_{dem} to the high power P_{HP} and the high energy battery part P_{HE}. From time 7050 s to 7125 s the power demand is being split to both battery parts. This leads to lower electrical losses within the battery parts due to the square dependency of electrical losses on the current ($\sim R_{\mathrm{dc}} \cdot I^2$). Furthermore the magnitude of high energy battery power P_{HE} corresponds to better dc-to-dc converter efficiency in comparison to partial-load operation with lower power. The recuperation phase in the second half of the figure shows that the regenerative energy is exclusively stored into the high power battery part. Hereby losses in the dc-to-dc converter can be avoided. On top of that, the high power battery is being re-charged during the driving cycle, what needs to be done to keep this battery part in a sort of charge-sustaining SoC range and to operate in a region of low inner resistance DCR, and an appropriate power capability respectively.

When comparing the two hybrid battery system topologies, it can be observed that the electrical losses within the dc-to-dc converter are reduced for topology 2, see figure 4. This is mainly because the absolute energy throughput of the high energy battery part for both topologies is bigger than that of the high power battery part. So less energy has to be transferred via dc-to-dc converter when operating topology 2.

A plot of the net energy throughput related to the C rate for the hybrid battery system topology at EoL condition is shown in figure 8. The limitation to a 1 C rate on the high energy battery part can be clearly

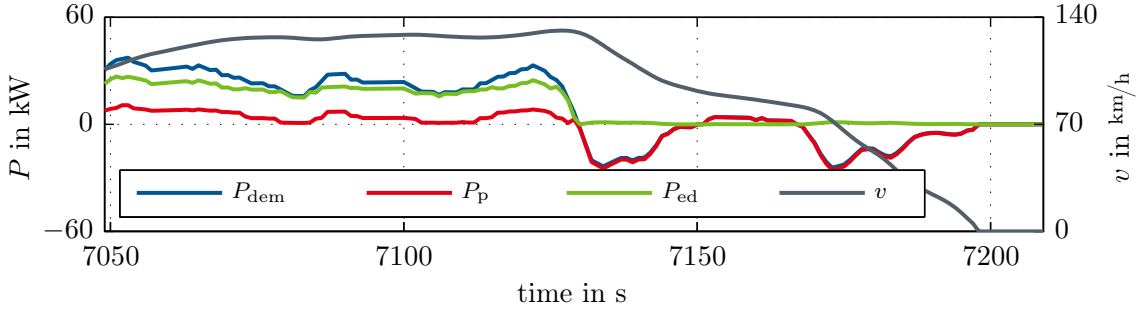

Figure 7: Extract of a Dynamic Programming result showing a high speed section, followed by a recuperation phase in the end. The power split between the high power (P_p) and the high energy (P_ed refers to the power at the dc-link) storage part is shown for hybrid battery system topology 1. P_dem refers to the demanded power at the dc-side of the inverter, corresponding to figure 3.

seen. Hence, the shift of peak loads to the high power battery part can be observed in figure 8b.

When comparing topology 1 with topology 2 at EoL condition the overall electrical energy losses increase in contrast to the BoL hybrid battery scenario. This is due to the fact that at EoL condition and with the chosen design the battery parts get nearly fully discharged over the 170 km driving distance and thus the load demand can not arbitrarily be shifted to the power battery. Hence additive losses in the high energy battery part, due to the increase of inner resistance, can not be avoided.

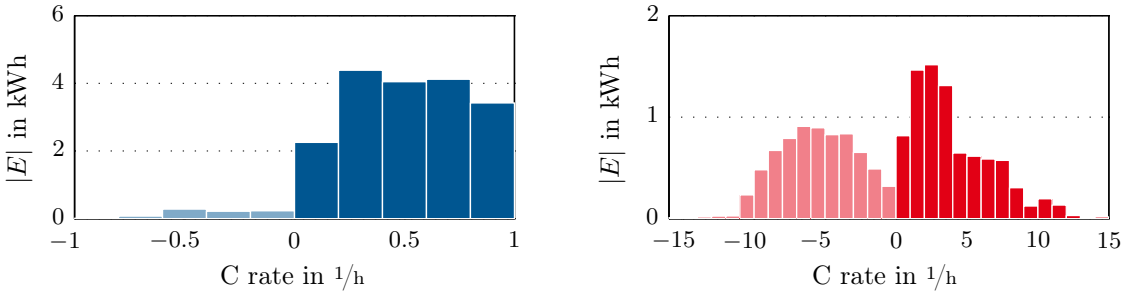

(a) High energy battery part

(b) High power battery part

Figure 8: Energy throughput on the battery parts of the hybrid battery system topology 1 for EoL condition of the high energy battery, related to the C rate (C rate > 0; Discharge).

5 Conclusion

A single-cell battery system and two hybrid battery system topologies for an electric vehicle application were compared in this work. The differences in terms of performance and energy efficiency for a high energy battery cell at begin of life and at end of life condition were analyzed. The investigated cells were characterized in the laboratory and the results were integrated into the simulation and optimization environment. A Dynamic Programming algorithm was applied on the optimal control problem of finding the energy optimal power trajectories for the hybrid battery system aiming at the objective to reduce the overall powertrain losses. The results show that the occurrence of high current rates on the energy battery cells can be reduced significantly for the hybrid battery system. Furthermore less overall net energy throughput is generated on the energy cells of the hybrid battery system topologies. These two findings are expected to enhance the lifetime of the high energy battery cells within the hybrid battery system. However when comparing the scenarios where a high energy cell at begin of life condition is used, the overall electrical energy losses in the powertrain are smaller for the single-cell battery system. This is mainly caused by the additive losses in the dc-to-dc converter for the hybrid battery system topologies. In contrast the energy efficiency gets worse for the single-cell battery system when comparing the scenarios where a cell in end of life condition is used. Furthermore the single-cell battery system shows an increase of net energy throughput at high C rates when operated with an aged battery cell. Besides additive losses this leads to higher heat generation within the cells. The hybrid battery system topologies may also allow the use of upcoming high energy battery cell chemistries that lack of power capability and lifetime.

References

[1] Ansarey, M. et al. “Optimal energy management in a dual-storage fuel-cell hybrid vehicle using multi-dimensional dynamic programming”. In: *Journal of Power Sources* 250 (2014), pp. 359–371.

[2] Araujo, R. E. et al. “Combined Sizing and Energy Management in EVs With Batteries and Supercapacitors”. In: *IEEE Transactions on Vehicular Technology*. Vol. 63, pp. 3062–3076.

[3] Bellman, R. *Dynamic Programming*. 1st ed. Princeton, USA: Princeton University Press, 1957.

[4] Bertsekas, D. P. *Dynamic Programming and Optimal Control*. 3rd edition. Belmont, USA: Athena Scientific, 1995.

[5] Bockstette, J. et al. “Bidirectional current controller for combination of different energy systems in HEV/EV”. In: *6th IET International Conference on Power Electronics, Machines and Drives*. 2012.

[6] Broussely, M. et al. “Main aging mechanisms in Li ion batteries”. In: *Journal of Power Sources* 146.1-2 (2005), pp. 90–96.

[7] Emadi, A. and Berthold, F. *Advanced electric drive vehicles*. Energy, power electronics, and machines. CRC Press, 2014.

[8] Fleurbaey, K. et al. “Analysis of Hybrid Rechargeable Energy Storage Systems in Series Plug-In Hybrid Electric Vehicles Based on Simulations”. In: *Energy and Power Engineering* 06.08 (2014), pp. 195–211.

[9] Föllinger, O. *Optimale Regelung und Steuerung*. 3., verb. Aufl. Methoden der Regelungs- und Automatisierungstechnik. München and Wien: Oldenbourg, 1994.

[10] Gao, L. et al. “Active power sharing in hybrid battery/capacitor power sources”. In: *18th Annual Applied Power Electronics Conference - APEC 2003*. 9-13 Feb. 2003, pp. 497–503.

[11] Garcia, O. “DC/DC-Wandler für die Leistungsverteilung in einem Elektrofahrzeug mit Brennstoffzellen und Superkondensatoren”. PhD thesis. 2002.

[12] Guzzella, L. and Sciarretta, A. *Vehicle Propulsion Systems*. Berlin, Heidelberg: Springer, 2013.

[13] Hartmann, N. and Özdemir, E. D. “Impact of different utilization scenarios of electric vehicles on the German grid in 2030”. In: *Journal of Power Sources* 196.4 (2011), pp. 2311–2318.

[14] Hentunen, A. et al. “Time-Domain Parameter Extraction Method for Thévenin-Equivalent Circuit Battery Models”. In: *IEEE Transactions on Energy Conversion* 29.3 (2014), pp. 558–566.

[15] Holland, C. E. et al. “Experimental characterization of hybrid power systems under pulse current loads”. In: *Journal of Power Sources* 109.1 (2002), pp. 32–37.

[16] International Organization for Standardization. *ISO 12405-2 Electrically propelled road vehicles - Test specification for lithium-ion traction battery packs and systems - Part 2: High-energy applications*. 2012-07-01.

[17] Koot, M. et al. “Energy management strategies for vehicular electric power systems”. In: *Vehicular Technology, IEEE Transactions on* 54.3 (2005), pp. 771–782.

[18] Ober-Blöbaum, S. “Discrete mechanics and optimal control”. PhD thesis. Universität Paderborn, 2008.

[19] Odeim, F. et al. “Power Management Optimization of a Fuel Cell / Battery / Supercapacitor Hybrid System for Transit Bus Applications”. In: *IEEE Transactions on Vehicular Technology* (2015).

[20] Omar, N. et al. “SuperLIB Project - Analysis of the performances of the hybrid lithium HE-HP architecture for plug-in hybrid electric vehicles”. In: *2013 World Electric Vehicle Symposium and Exhibition (EVS27)*. 2013, pp. 1–10.

[21] Onda, K. et al. “Thermal behavior of small lithium-ion battery during rapid charge and discharge cycles”. In: *Journal of Power Sources* 158.1 (2006), pp. 535–542.

[22] Roscher, M. “Zustandserkennung von $LiFePO_4$-Batterien für Hybrid- und Elektrofahrzeuge”. PhD thesis. Aachen: Rheinisch-Westfälisch Technische Hochschule Aachen.

[23] Rothgang, S. et al. “HV Traction Battery: From Layout to Realization”. In: *World Electric Vehicle Journal* 5 (2012), pp. 176–185.

[24] Rothgang, S. et al. “Modular battery design for reliable, flexible and multi-technology energy storage systems”. In: *Applied Energy* 137 (2015), pp. 931–937.

[25] Schmidt, H. “Worldwide Harmonized Light-Vehicles Test Procedure (WLTP) und Real Driving Emissions (RDE) - aktueller Stand der Diskussion und erste Messergebnisse”. In: *15. Internationales Stuttgarter Symposium*. 2015, pp. 1403–1411.

[26] Schmidt, J. P. “Verfahren zur Charakterisierung und Modellierung von Lithium-Ionen Zellen”. PhD thesis. Karlsruhe, 2013.

[27] Schoenen, T. “Einsatz eines DC-DC-Wandlers zur Spannungsanpassung zwischen Antrieb und Energiespeicher in Elektro- und Hybridfahrzeugen”. PhD thesis. Aachen: Rheinisch-Westfälisch Technische Hochschule Aachen, 2011.

[28] Simmons, K. et al. “Modeling and energy management control design for a fuel cell hybrid passenger bus”. In: *Journal of Power Sources* 246 (2014), pp. 736–746.

[29] Sundström, O. and Guzzella, L. “A generic dynamic programming Matlab function”. In: *Control Applications, (CCA) Intelligent Control, (ISIC), 2009 IEEE*. 2009, pp. 1625–1630.

[30] Sundström, O. et al. “On Implementation of Dynamic Programming for Optimal Control Problems with Final State Constraints”. In: *Oil & Gas Science and Technology (Oil & Gas Science and Technology - Revue de l’Institut Français du Pétrole)* 65.1 (2010), pp. 91–102.

[31] Verband der Automobilindustrie e. V. *Test specification for lithium-ion battery systems for hybrid electric vehicles*. 5.03.2007.

[32] Vetter, J. et al. “Ageing mechanisms in lithium-ion batteries”. In: *Journal of Power Sources* 147.1-2 (2005), pp. 269–281.

Authors

Raphael Wegmann received his Master of Science degree in Electrical Engineering from RWTH Aachen University, Germany. In 2014 he joined the Robert Bosch GmbH as a research associate. His areas of interest are hybrid battery systems for automotive and non-automotive applications.

Volker Döge studied physics at the Technical University of Braunschweig and received its PhD in physical chemistry in the year 1996. Since 1993 he was active in secondary lithium and capacitor development projects within the FhG ICT, FORTU BAT Batteries GmbH and EPCOS AG. In the year of 2006 he joined Bosch working in the field of lithium battery development and research, since 2009 within the corporate research business sector focusing on mobile and automotive systems.

Dirk Uwe Sauer received his diploma in Physics from University of Darmstadt in 1994. From 1994 to 2003 he worked at Fraunhofer ISE as a research scientist, from 2000-2003 as team leader for Storage Systems. After receiving his PhD from University of Ulm in 2003, topic: ”Optimisation the usage of lead-acid batteries in photovoltaic-hybrid systems with special emphasis on battery aging”, he joined ISEA as professor for Electrochemical Energy Conversion and Storage Systems.